Springer

KSME

Journal of Mechanical Science and Technology 28 (2) (2014) 581~593
www.springerlink.com/content/1738-494x
DOI 10.1007/s12206-013-1191-7

An optimization approach for black-and-white and hinge-removal topology designs †

Yongqing Fu[1] and Xianmin Zhang[2,*]

[1]*School of Design, South China University of Technology, Guangzhou, Guangdong 510640, China*
[2]*School of Mechanical and Automotive Engineering, South China University of Technology, Guangzhou, Guangdong 510640, China*

(Manuscript Received May 4, 2012; Revised March 20, 2013; Accepted October 3, 2013)

Abstract

An optimization approach for black-and-white and hinge-removal topology designs is studied. To achieve this motive, an optimal topology allowing grey boundaries is found firstly. When a suitable design has been obtained, this solution is then used as a starting point for the follow-up optimization with the goal to free unfavorable intermediate elements. For this purpose, an updated optimality criterion in which a threshold factor is introduced to gradually suppress elements with low density is proposed. The typical optimality method and new technique proposed are applied to the design procedure sequentially. Besides, to circumvent the one-point hinge connection problem producing in the process of freeing intermediate elements, a hinge-removal strategy is also proposed. During the optimization, the binary constraints on design variables are relaxed based on the scheme of solid isotropic material with penalization. Meanwhile, the mesh-independency filter is employed to ensure the existence of a solution and remove well-known checkerboards. In this way, a solution that has few intermediate elements and is free of one-point hinge connections is obtained. Finally, different numerical examples including the compliance minimization, compliant mechanisms and vibration problems demonstrate the validity of the proposed approach.

Keywords: Black-and-white and hinge-removal topology designs; Hinge-removal strategy; Threshold factor; Topology optimization; Updated optimality criterion

1. Introduction

By means of the method of topology optimization, general topology optimization problems, such as the compliance minimization, compliant mechanisms and vibration problems, can be posed as material distribution problems. During the process of solving, the design domain is usually divided into a certain number of finite elements. Subsequently, to determine the optimal placement of a given isotropic material in the design space, a numerical optimization cycle is needed. For reasons of the manufacture, a black-and-white (0-1) structural topology is classically desired, whereas it requires mathematical programming that can handle lots of discrete 0-1 design variables, such as simulated annealing [1, 2], genetic algorithm [3, 4], sequential integer programming methods [5, 6], dual method [7, 8], and methods for global optimization [9, 10], and so on. However, it is computationally prohibitive to solve the optimum problem using these methods. Thus, the most common approach to circumvent solution difficulties is still to relax design variables, i.e. replace the integer variables with continuous variables [11-21], so that the material distribution problem can be solved using most mathematical programming with continuous design variables. Among the relaxation methods, two major approaches, namely microstructure based and power law based, are used in the field of the topology optimization. The homogenization technique [11, 12], which determines the optimal material distribution by designing the size parameters of microstructures, is a representative microstructure method. This technique is effective for a large class of elasticity problems, but it commonly needs a lot of design variables and results in topologies with micro perforations, checkerboards and one-point hinge connections. As an alternative, SIMP (solid isotropic material with penalization) method has thereby become increasingly popular due to its advantages in computation efficiency and conception simplicity. This method directly treats the material density of each element as a design variable, which reduces the size of the optimization problem to a large extent [13-19], whereas it is noteworthy that the SIMP method could produce topologies with intermediate elements. It is very impractical and of high cost to produce structural elements with varied densities. This means that the intermediate values of this artificial material model should be penalized in some manner to make them uneconomical. In past works, researchers usually ensured continuous design variables to be forced towards a black and white solution by applying a penalization on the density of element as ρ^p, ($p > 1$) [13-18]. But this penalization method is

*Corresponding author. Tel.: +86 2087110059, Fax.: +86 2087110059
E-mail address: zhangxm@scut.edu.cn
† Recommended by Associate Editor Jeonghoon Yoo

prone to lead to checkerboards and one-point hinge connections. This necessitates applications of some restriction methods, such as the perimeter [22], local gradient [23] and mesh-independency filter [24, 25]. By exerting a length scale on the variable variation, these methods can make checkerboards and one-point hinge connections to be arbitrarily weak, but grey band could thus be brought around the topology again, as reviewed in Refs. [20] and [26]. Another method is to employ a specified threshold value to obtain elements with normalized densities equivalent to either 1.0 or 0.0 [27, 28]. However, it is not evident how to choose the threshold value appropriately in these works. In order to relieve intermediate elements in the resultant topologies, explicit penalization terms are also proposed to either append to the objective function [29] or impose as a separate constraint [30]. However, it is also possible for the extra penalization terms to cause difficulties for the optimization software in finding a feasible solution. In addition to the above methods, other methods include a simple heuristic for gray-scale suppression by the modification of the optimality criterion statement by Groenwold et al. [19], a method combing a separate constraint and a post-processor based on the sequential linear integer programming by Werme [31], filtering techniques based on image processing by Sigmund [32] and Wang et al. [33], a hybrid SINH method by Bruns [34], evolutionary structural optimization method by Chu et al. [35], complex-shaped beam element and graph-based optimization by Sauter et al. [36], A hybrid methodology combining simulated annealing and SIMP by Garcia-Lopez et al. [37], standardized elements by Jang et al. [38], curve-based methods by Luo et al. [39], James et al. [40], Wang et al. [41] and Zhou et al. [42].

In this paper, an optimization approach for black-and-white and hinge-removal topology designs is studied. To achieve this motive, an optimal topology allowing grey boundaries is found firstly. When a suitable design has been obtained, this solution is then used as a starting point for the follow-up optimization with the goal to free unfavorable intermediate elements. For this purpose, an updated optimality criterion in which a threshold factor is introduced to gradually suppress elements with low density is proposed. The typical optimality method and new technique proposed are applied to the design procedure sequentially. Besides, to circumvent the one-point hinge connection problem producing in the process of freeing intermediate elements, the hinge-removal strategy is also proposed. During the optimization, the binary constraints on design variables are relaxed based on the scheme of solid isotropic material with penalization. Meanwhile, the mesh-independency filter is employed to ensure the existence of a solution and remove well-known checkerboards. In this way, a solution that has few intermediate elements and is free of one-point hinge connections is obtained. Finally, different numerical examples including the compliance minimization, compliant mechanisms and vibration problems demonstrate the validity of the proposed approach.

2. Basic notation and problem formulation of test problems

2.1 Basic notation

Assume that the design domain Ω is discretized into N finite elements. Element densities $\rho_e,\ e=1,2,\cdots,N$ are considered as design variables. The bounds of $\rho_e,\ e=1,2,\cdots,N$ are

$$\rho_e \in [\rho_{\min},1] \qquad (e=1,2,\cdots,N) \tag{1}$$

where $\rho_{\min}$ is a positive lower bound and taken the value of 0.001 here, whose function is to prevent the singularity of the finite element stiffness matrix. As a result, the element stiffness matrix $\boldsymbol{K}_e$ should vary with the element density variable ρ_e and can be expressed as [17]:

$$\boldsymbol{K}_e = \rho_e^p \boldsymbol{K}^0 \qquad (p \in Z, p>1) \tag{2}$$

where penalization factor p is used to enforce extreme values of design variables. In the present approach, the penalty parameter p is fixed at $p=3$ to hasten the optimization convergence, $\boldsymbol{K}^0$ is the stiffness matrix of an arbitrary solid element and can be written as:

$$\boldsymbol{K}^0 = \int_{V_e} \boldsymbol{B}^T \boldsymbol{D}\boldsymbol{B} dV \tag{3}$$

where V_e is the material volume of a solid element, $\boldsymbol{B}$ is the strain matrix of a point of a solid element. On the other hand, the element mass matrix $\boldsymbol{M}_e$ in the vibration problem is also the function of the element density and can be written as:

$$\boldsymbol{M}_e = \rho_e^q \boldsymbol{M}^0 \tag{4}$$

where q is a penalization factor, normally $q=1$ is chosen [43], $\boldsymbol{M}^0$ represents the element mass matrix of an arbitrary solid element and can be written by using the shape function matrix $\boldsymbol{N}_s$ and the material density ρ_{mat} as:

$$\boldsymbol{M}^0 = \int_{V_e} \rho_{\text{mat}} \boldsymbol{N}_s^T \boldsymbol{N}_s dV. \tag{5}$$

Note that localized eigenmodes may occur in subregions of the design domain with low values of the material density (e.g., $\rho_e \le 0.1$) [43, 44]. For this reason, $\boldsymbol{M}_e$ is thus rewritten as [43]:

$$\boldsymbol{M}_e = \begin{cases} \rho_e \boldsymbol{M}^0 & (\rho_e > 0.1) \\ 10^5 \rho_e^6 \boldsymbol{M}^0 & (\rho_e \le 0.1). \end{cases} \tag{6}$$

From Eqs. (2) and (6), the global stiffness matrix $\boldsymbol{K}$ and mass matrix $\boldsymbol{M}$ can be formulated as:

$$\boldsymbol{K} = \sum_e \boldsymbol{K}_e, \quad \boldsymbol{M} = \sum_e \boldsymbol{M}_e \tag{7}$$

2.2 Problem formulation of test problems

In this paper, the compliance minimization problems, compliant mechanism problems and fundamental eigenvalue problems are respectively employed to test the feasibility of the proposed algorithm. In what follows, the corresponding problem formulations will be presented.

2.2.1 Compliance minimization problems

Under given load $\boldsymbol{F}_{\text{in}}$ and boundary conditions, the problem formulation with the objective to minimize compliance can be written as:

$$\begin{cases} \text{Min} \quad E_s(\boldsymbol{\rho}) = \boldsymbol{F}^T\boldsymbol{U} \\ \text{s.t.} \quad \boldsymbol{K}\boldsymbol{U} = \boldsymbol{F} \\ \quad \sum_e V_e\rho_e \le \theta V^0 \\ \quad 0 < \rho_{\min} \le \rho_e \le \rho_{\max} = 1, \quad e = 1,2,\cdots,N \end{cases} \tag{8}$$

where $\boldsymbol{\rho}$ is a column vector constructed by ρ_e, $e = 1,2,\cdots,N$, $\rho_{\max}$ is the upper bound of design variable ρ_e and taken the value of 1, $\boldsymbol{U}$ is the nodal displacement vector, $\boldsymbol{F}$ is the force vector with zeros at all degrees of freedom except at the input point where it is $\boldsymbol{F}_{\text{in}}$, θ and V^0 are respectively the volume fraction and total volume of the design domain, E_s is the strain energy of the compliance minimization problem.

2.2.2 Compliant mechanism problems

A compliant mechanism should be flexible so that it can easily deform to achieve given mission, but it should also be stiff to provide an adequate mechanical advantage and working stability [20, 21, 45]. Usually, the strain energy and mutual potential energy are respectively formulated as measures for the overall stiffness and flexibility of a compliant mechanism. Assuming that active load $\boldsymbol{F}_{\text{in}}$ is specified, again assuming unit dummy load $\boldsymbol{F}_{\text{out}}$ is applied at output point in the direction of the output displacement, the compliant mechanism problem can be defined in terms of these two conflicting objectives as [45-51]

$$\begin{cases} \text{Min} \quad f_{sm}(\boldsymbol{\rho}) = -\dfrac{E_{ms}}{E_s} \\ \text{s.t.} \quad \boldsymbol{K}\boldsymbol{U} = \boldsymbol{F} \\ \quad \boldsymbol{K}\boldsymbol{U}^d = \boldsymbol{F}^d \\ \quad \sum_e V_e\rho_e \le \theta V^0 \\ \quad 0 < \rho_{\min} \le \rho_e \le \rho_{\max} = 1, \quad e = 1,2,\cdots,N \end{cases} \tag{9}$$

where F^d is the force vector with zeros at all degrees of freedom except at the output point where it is $\boldsymbol{F}_{\text{out}}$, $\boldsymbol{U}^d$ is the nodal displacement vector under the load $\boldsymbol{F}_{\text{out}}$, E_{ms} is the mutual potential energy and can be formulated as:

$$E_{ms} = (\boldsymbol{F}^d)^T\boldsymbol{U}. \tag{10}$$

2.2.3 Eigenvalue problems

For dynamically loaded structures, a commonly used design goal is to maximize the fundamental eigenvalue $\lambda_{\min}$, which can be formulated as [20, 43, 44]:

$$\begin{cases} \text{Max}\left\{\lambda_{\min} = \min\limits_{j=1,2,\cdots,J} \lambda_j\right\} \\ \text{s.t.} \quad \boldsymbol{K}\boldsymbol{\Phi}_j = \omega_j^2\boldsymbol{M}\boldsymbol{\Phi}_j, \quad j = 1,2,\cdots,J \\ \quad \sum_e V_e\rho_e \le \theta V^0 \\ \quad 0 < \rho_{\min} \le \rho_e \le \rho_{\max} = 1, \quad e = 1,2,\cdots,N \end{cases} \tag{11}$$

where $\boldsymbol{M}$ is the global mass matrix, λ_j and ω_j are respectively the j *th* eigenvalue and eigenfrequency with $\lambda_j = \omega_j^2$, $\boldsymbol{\Phi}_j$ is the eigenvector corresponding to ω_j, and $\boldsymbol{\Phi}_j$, $j = 1,2,\cdots,J$ are $\boldsymbol{M}$ orthonormalized. Simultaneously, all the J candidate eigenvalues considered should be numbered such that

$$0 < \lambda_1 < \lambda_2 < \cdots < \lambda_{J-1} < \lambda_J. \tag{12}$$

Moreover, for the problem Eq. (11), concentrated nonstructural masses are added to parts of the design domain to avoid trivial solutions during the solving process [20, 43].

3. The hinge-removal strategy

When forcing continuous design variables towards a black and white solution, the one-point hinge connection problem may be encountered, which leads to the connection of zero thickness, as plotted in Fig. 1. This makes the designed compliant mechanism not to be suited for manufacture from one piece of material. To circumvent this problem, the hinge-removal strategy is proposed in the present study. Specifically, at the beginning of each optimization iteration, one-point hinge connection patches in the topology are firstly checked. Consider the patch of four contiguous elements e_{11}, e_{21}, e_{31} and e_{41} and define the following condition

$$\begin{cases} \rho_{e_{11}} \le \delta_1 \\ \rho_{e_{21}} \le \delta_1 \\ \rho_{e_{31}} \ge \delta_2 \\ \rho_{e_{41}} \ge \delta_2 \end{cases} \tag{13}$$

where δ_1 and δ_2 are predetermined hinge detection parameters with $\delta_1 < \delta_2$, $\rho_{e_{11}}$, $\rho_{e_{21}}$, $\rho_{e_{31}}$ and $\rho_{e_{41}}$ are respectively densities of elements e_{11}, e_{21}, e_{31} and e_{41}. If the condition in Eq. (13) holds true, one can determine that elements e_{11}, e_{21}, e_{31} and e_{41} constitute a potential patch of the one-point hinge connection, as shown in Fig. 1(a) or Fig. 1(b). Of these, elements e_{11} and e_{21} are ones with relatively low density, while elements e_{31} and e_{41} are ones with relatively high density. In order to cure the hinge patch checked, densities of elements e_{11} and e_{21} are then modified by using ones of elements e_{31} and e_{41} as

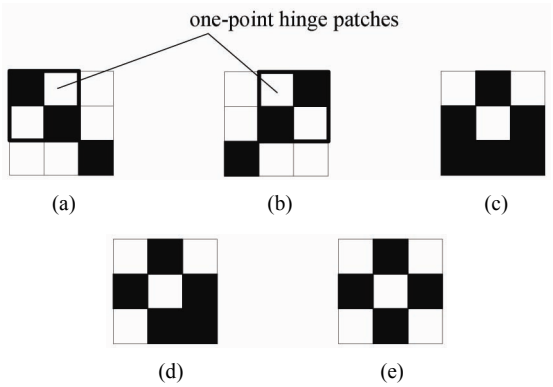

Fig. 1. The cases of one-point hinge connection: (a) $H = 1$; (b) $H = 1$; (c) $H = 1$ and $H = 2$; (d) $H = 1$ and $H = 3$; (e) $H = 1$ and $H = 4$.

$$\hat{g}(\rho_e) = \frac{1}{2}(\rho_{e_{31}} + \rho_{e_{41}}) \tag{14}$$

where $\hat{g}(\rho_e)$ is the modified density of element e, e respresents low-density element e_{11} or e_{21} possessed by a potential one-point hinge patch. To including all cases shown in Figs. 1(c)-(e), Eq. (14) is thus rewritten as:

$$g(\rho_e) = \frac{1}{H}\sum_{h=1}^{H}(\hat{g}(\rho_e))_h \tag{15}$$

where $g(\rho_e)$ is the modified density of low-density element e possessed by the H $(1 \le H \le 4)$ potential one-point hinge patches, h is the number of the one-point hinge patch.

4. Numerical implementation

For simplicity, assume that Ω_{dl} is the set of the elements with relatively low density in all patches of the one-point hinge connection in the design domain. One can define the modified density of element e of set $\Omega\backslash\Omega_{dl}$ as:

$$g(\rho_e) = \rho_e \qquad e \in \Omega \setminus \Omega_{dl}\ . \tag{16}$$

For all elements in the design domain, the modified densities Eqs. (15) and (16) are used to replace the original values in the stiffness matrix $\boldsymbol{K}$ and mass matrix $\boldsymbol{M}$. Hence, sensitivities of the objective functions of the above optimization problems with respect to design variable ρ_i can respectively be represented as [20, 33, 43, 44]:

$$\frac{\partial E_s}{\partial \rho_i} = -\sum_{e=1}^{N} p(g(\rho_e))^{p-1}\frac{\partial g(\rho_e)}{\partial \rho_i}(\boldsymbol{u}_e)^T \boldsymbol{K}^0 \boldsymbol{u}_e \tag{17}$$

$$\frac{\partial f_{sm}}{\partial \rho_i} = \sum_{e=1}^{N}\frac{1}{(E_s)^2}\left(E_s p(g(\rho_e))^{p-1}\frac{\partial g(\rho_e)}{\partial \rho_i}(\boldsymbol{u}_e)^T \boldsymbol{K}^0 \boldsymbol{u}_e^d - E_{ms} p(g(\rho_e))^{p-1}\frac{\partial g(\rho_e)}{\partial \rho_i}(\boldsymbol{u}_e)^T \boldsymbol{K}^0 \boldsymbol{u}_e \right) \tag{18}$$

$$\frac{\partial \lambda_j}{\partial \rho_i} = -\sum_{e=1}^{N}(\boldsymbol{\Phi}_{je})^T\left(p(g(\rho_e))^{p-1}\frac{\partial g(\rho_e)}{\partial \rho_i}\boldsymbol{K}^0 - \lambda_j q(g(\rho_e))^{q-1}\frac{\partial g(\rho_e)}{\partial \rho_i}\boldsymbol{M}^0\right)\boldsymbol{\Phi}_{je} \tag{19}$$

where $\boldsymbol{u}_e$ and $\boldsymbol{u}_e^d$ are the nodal displacement vectors of element e due to $\boldsymbol{F}_{\text{in}}$ and $\boldsymbol{F}_{\text{out}}$ respectively, $\boldsymbol{\Phi}_{je}$ is eigenvector of element e, $\partial g(\rho_e)/\partial \rho_i$ is the sensitivity of the modified density $g(\rho_e)$ with respect to design variable ρ_i. For element e of set Ω_{dl}, one obtained

$$\frac{\partial g(\rho_e)}{\partial \rho_i} = \frac{1}{H}\left(\sum_{h=1}^{H}\frac{\partial(\hat{g}(\rho_e))_h}{\partial \rho_i}\right). \tag{20}$$

Considering the common high-density elements possessing by any two one-point hinge patches among the H ones, Eq. (20) can be further written as:

$$\frac{\partial g(\rho_e)}{\partial \rho_i} = \begin{cases} 1/2 & \text{if } H = 1,\ i \in S_{11} \\ 1/2 & \text{if } H = 2,\ i \in S_{21} \\ 1/4 & \text{if } H = 2,\ i \in S_{22} - S_{21} \\ 1/3 & \text{if } H = 3,\ i \in S_{31} \\ 1/6 & \text{if } H = 3,\ i \in S_{32} - S_{31} \\ 1/4 & \text{if } H = 4,\ i \in S_{41} \\ 0 & \text{otherwise} \end{cases} \tag{21}$$

where sets S_{11}, S_{21}, S_{22}, S_{31}, S_{32} and S_{41} can be formulated as

$$S_{11} = \{e_{31}, e_{41}\} \tag{22}$$

$$S_{21} = \{e_{31}, e_{41}\} \cap \{e_{32}, e_{42}\} \tag{23}$$

$$S_{22} = \{e_{31}, e_{41}\} \cup \{e_{32}, e_{42}\} \tag{24}$$

$$S_{31} = (\{e_{31}, e_{41}\} \cap \{e_{32}, e_{42}\}) \cup (\{e_{31}, e_{41}\} \cap \{e_{33}, e_{43}\}) \cup (\{e_{32}, e_{42}\} \cap \{e_{33}, e_{43}\}) \tag{25}$$

$$S_{32} = \{e_{31}, e_{41}\} \cup \{e_{32}, e_{42}\} \cup \{e_{33}, e_{43}\} \tag{26}$$

$$S_{41} = \{e_{31}, e_{41}\} \cup \{e_{32}, e_{42}\} \cup \{e_{33}, e_{43}\} \cup \{e_{34}, e_{44}\} \tag{27}$$

where e_{3h} and e_{4h} are elements with relatively high density in the h *th* one-point hinge patch of element e. And for element e of set $\Omega\backslash\Omega_{dl}$, one has

$$\frac{\partial g(\rho_e)}{\partial \rho_i} = \begin{cases} 1 & \text{if } i = e \\ 0 & \text{otherwise}\ . \end{cases} \tag{28}$$

Moreover, the sensitivity of the volume constraint can be written as:

$$\frac{\partial V(\boldsymbol{\rho})}{\partial \rho_i} = \frac{\partial\left(\sum_e V_e \rho_e\right)}{\partial \rho_i} = V_e \tag{29}$$

where $V(\rho)$ is the volume of the optimized topology. Clearly, the emergence of the one-point hinge patch will lead to an increase in the complexity of the sensitivity calculation of the objective function. Nevertheless, by using the hinge-removal strategy proposed, one-point hinge connections can be found and circumvented promptly, which avoids the reproducing of this problem in the same location in subsequent iterations. Moreover, considering that the one-point hinge problem often produces in the process of freeing intermediate elements, the hinge-removal strategy will be implemented only in the follow-up optimization. Further, δ_1 is chosen as a small value for most cases in this work such that a smaller number of potential one-point hinge connections can be expected. As a result, computational effort on the cure of the one-point hinge problem would be greatly reduced. Especially for the case where no one-point hinge connection is found, the implementation of the hinge-removal strategy has little influence on the CPU time. Therefore, the proposed hinge-removal strategy will be applied in the three problems mentioned above.

5. Optimality criterion

5.1 Typical optimality criterion

In the proposed approach, an optimal topology with grey boundaries is found firstly. Therefore, the typical optimality criterion (OC) method with continuous design variables is employed to update element densities. Following Bendsøe and Sigmund [20] and considering the hinge-removal strategy, a heuristic updating scheme for density variables in the above design problems can be formulated as:

$$\rho_e^{k+1}=\begin{cases}(g(\rho_e))^k(\Lambda_e^k)^\eta \\ \quad \text{if} \quad \max\left\{(1-\zeta)(g(\rho_e))^k,\rho_{\min}\right\} \\ \quad\quad <(g(\rho_e))^k(\Lambda_e^k)^\eta \\ \quad\quad <\min\left\{(1+\zeta)(g(\rho_e))^k,\rho_{\max}\right\} \\ \min\left\{(1+\zeta)(g(\rho_e))^k,\rho_{\max}\right\} \\ \quad \text{if} \quad (g(\rho_e))^k(\Lambda_e^k)^\eta \\ \quad\quad \geq \min\left\{(1+\zeta)(g(\rho_e))^k,\rho_{\max}\right\} \\ \max\left\{(1-\zeta)(g(\rho_e))^k,\rho_{\min}\right\} \\ \quad \text{if} \quad (g(\rho_e))^k(\Lambda_e^k)^\eta \\ \quad\quad \leq \max\left\{(1-\zeta)(g(\rho_e))^k,\rho_{\min}\right\}\end{cases} \tag{30}$$

where k is the iteration number, η $(0<\eta<1)$ is a relaxation factor, ζ is a small move limit, and Λ_e^k is non-negative and written as [20]:

$$\Lambda_e^k=\max(0,B_e^k) \tag{31}$$

where B_e^k are found from the Kuhn-Tucker necessary conditions as [20]:

$$B_e^k=\frac{-\left(\dfrac{\partial f}{\partial \rho_e}\right)^k}{\gamma^k\dfrac{\partial V}{\partial \rho_e}} \tag{32}$$

where $\partial f/\partial\rho_e$ is the sensitivity of the overall objective function in Eqs. (17) − (19), γ is a Lagrange multiplier, which is adjusted by a bi-sectioning algorithm iteration in OC to ensure $\boldsymbol{\rho}^{k+1}$ in Eq. (30) to satisfy the active volume constraint, i.e. [20, 52-55]

$$\begin{aligned}&\theta V^0-\Big\{\textstyle\sum_{icas1}V_e(g(\rho_e))^k(\Lambda_e^k)^\eta \\ &+\textstyle\sum_{icas2}V_e\min\left\{(1+\zeta)(g(\rho_e))^k,\rho_{\max}\right\} \\ &+\textstyle\sum_{icas3}V_e\max\left\{(1-\zeta)(g(\rho_e))^k,\rho_{\min}\right\}\Big\}=0\end{aligned} \tag{33}$$

where $\sum_{icas1}$, $\sum_{icas2}$ and $\sum_{icas3}$ are sums of three types of design variables updated in Eq. (30), respectively.

5.2 Updated optimality criterion

When a suitable design allowing grey boundaries has been obtained, the optimal solution is then used as a starting point for the follow-up optimization with the goal to free unfavorable intermediate elements, such that desired black-and-white topology can be obtained. For this reason, an updated optimality criterion is developed by slightly modifying OC in Eq. (30) to update density variables. The updated optimality criterion is written as:

$$\rho_e^{k+1}=\begin{cases}\rho_{\max} \quad \text{if} \quad (g(\rho_e))^k=\rho_{\max} \\ \min\left\{(1+\zeta)(g(\rho_e))^k,\rho_{\max}\right\} \\ \quad \text{else if} \quad (g(\rho_e))^k(\Lambda_e^k)^\eta \\ \quad\quad \geq \min\left\{(1+\zeta)(g(\rho_e))^k,\rho_{\max}\right\} \\ (g(\rho_e))^k(\Lambda_e^k)^\eta \\ \quad \text{else if} \quad \alpha\leq(g(\rho_e))^k(\Lambda_e^k)^\eta \\ \quad\quad <\min\left\{(1+\zeta)(g(\rho_e))^k,\rho_{\max}\right\} \\ \rho_{\min} \quad \text{otherwise}\end{cases} \tag{34}$$

where parameter α is a threshold factor, and $\rho_{\min}<\alpha\leq 1$, the function of which is to inhibit elements with intermediate densities. The reasons to adopt Eq. (34) as an updated criterion include the following aspects. Firstly, because the optimal topology with grey boundaries is used as an initial design for the follow-up optimization, what should be removed are only intermediate elements. Thus, during the k+1 *th* iteration, those elements whose densities are $\rho_{\max}$ in the k *th* iteration remain unchanged. Secondly, from the stiffness matrix and mass ma-

trix of the finite element, it can be seen that elements with high density have larger contribution to the design problem than the ones with low densities. Therefore, elements with $g(\rho_e)^k(\Lambda_e^k)^\eta < \alpha$ are deleted; and elements with $\alpha \le (g(\rho_e))^k(\Lambda_e^k)^\eta < \min\left\{(1+\zeta)(g(\rho_e))^k, \rho_{\max}\right\}$ are updated by $(g(\rho_e))^k(\Lambda_e^k)^\eta$; while elements with $(g(\rho_e))^k(\Lambda_e^k)^\eta \ge \min\left\{(1+\zeta)(g(\rho_e))^k, \rho_{\max}\right\}$ are updated by $\min\left\{(1+\zeta)(g(\rho_e))^k, \rho_{\max}\right\}$. Thirdly, By virtue of inhibiting the appearance of elements with $(g(\rho_e))^k(\Lambda_e^k)^\eta < \alpha$, material can be added to the high-density elements as expected. Further, in order to obtain a preferable effect to remove intermediate elements, a continuation scheme similar to that developed by Sigmund [32] is thus used to determine parameter α in this study. That is, parameter α should be specified as a relatively small positive number initially and then increased gradually during the iteration until that the ideal 0-1 topology is obtained. Of course, it should also be noted here that for the continuation scheme a relatively large iteration number to achieve convergence may be required, as observed in Ref. [32]. However, because of the easy formulation by slightly modifying OC, the updated optimality criterion itself doesn't increase the complexity of the sensitivity calculation of the objective function. By integrating the hinge-removal strategy with the updated optimality criterion, it can be seen that the proposed approach only requires calculation complexity as low as possible. The increase in the CPU time with the present optimization approach would thus be moderate. From this perspective, the proposed approach is meaningful and feasible for black-and-white and hinge-removal topology designs.

6. Sensitivity filter

During the whole optimization process, in order to ensure the existence of a solution and remove the well-known checkerboards, we employed the popular mesh-independency filter, which works by modifying the element sensitivities as [25]:

$$\frac{\partial \hat{f}}{\partial \rho_i} = \frac{1}{\rho_i \sum_{e\in NE_i} \hat{H}_e} \sum_{e\in NE_i} \hat{H}_e \rho_e \frac{\partial f}{\partial \rho_e} \qquad i = 1,\ldots,N \tag{35}$$

where NE_i is the neighborhood of element i, which is defined by the elements having centers within a given filter radius R of the center of element i. Let $\boldsymbol{x}_e$ is the center location of element e, one has [25]

$$NE_i = \left\{e \middle| \left\|\boldsymbol{x}_e - \boldsymbol{x}_i\right\| \le R\right\} \tag{36}$$

And $\hat{H}_e$ is a convolution operator decaying linearly with the distance from element i, i.e. [25]

$$\hat{H}_e = R - \left\|\boldsymbol{x}_e - \boldsymbol{x}_i\right\| \tag{37}$$

During the whole optimization, the modified sensitivities Eq. (35) are used to replace the original values in Eqs. (17) – (19).

7. Optimization procedure

The algorithm of the proposed approach for black-and-white topology design of compliant mechanisms can be formulated in the following way.

1: Initialize the initial and follow-up density variables $\boldsymbol{\rho}_{\text{fir}}$ and $\boldsymbol{\rho}_{\text{sec}}$, the initial value α_0 and increment $\Delta\alpha$ of threshold factor α, the initial iteration number N_1, iteration number N_2, iteration counter k, hinge detection parameters δ_1 and δ_2, the maximum change $d_{\max}$ in design variables $\boldsymbol{\rho}_{\text{sec}}$, intermediate element counter N_g, the filtering radius R and the stopping limit ε.

2: Modify iteration counter k.

3: If $k = N_1+1$, then $\boldsymbol{\rho}_{\text{sec}}=\boldsymbol{\rho}_{\text{fir}}$.

4: If $k > N_1$ is true, perform the hinge-removal strategy.

5: Perform finite element analysis, sensitivity calculation and mesh-independency filter.

6: If $k \le N_1$ is true, update design variables $\boldsymbol{\rho}_{\text{fir}}$ based on the typical OC in Eq. (30). Otherwise, perform the continuation scheme similar to that in Ref. [32], i.e.

if abs($V(\boldsymbol{\rho})/V^0 - \theta$) ≤ 0.0001 and mod(k,N_2)==1 then

$\alpha = \alpha + \min(\Delta\alpha, 1-\alpha)$

end

and update design variables $\boldsymbol{\rho}_{\text{sec}}$ based on the updated OC in Eq. (34).

7: If $k \le N_1$ is true, repeat steps 2-7.

8: If $d_{\max} \le \varepsilon$ and $k > N_1$ is true, calculate $V(\boldsymbol{\rho})$ and N_g. Otherwise, repeat steps 2-8.

9: Modify ε according to the values of $V(\boldsymbol{\rho})$ and N_g. Repeat steps 2-9 until a solution with volume preserving and few intermediate elements is obtained.

In this algorithm, when giving α_0 and $\Delta\alpha$, the termination value of α is adjusted implicitly by the modification of ε to avoid difficulty in specifying it artificially. More specifically, a decrease in ε will lead to an increase in the termination value of α, which will bring a better black-and-white solution. Based on numerical experience, parameter ε can take the value of $1e-\vartheta$ (where ϑ is a positive integer) and be modified as follows: if there exist intermediate elements in the final topology adhering to the volume constraint, which indicates that the termination value of α is too small, one should attempt to decrease ε appropriately. With this implicit adjustment, desired black-and-white topology design satisfying the volume constraint can be obtained. On the other hand, hinge detection parameter δ_2 ideally takes the value of 1 to ensure the continuity of the resultant material. Also, computational experience shows that purely black-and-white topologies are often obtained with $\vartheta \ge 6$, so parameter ε is initialized as $1e-2$ to ensure an increasing α in seeking the optimum solution in this study.

In a sum, the flowchart of the proposed approach is given in Fig. 2.

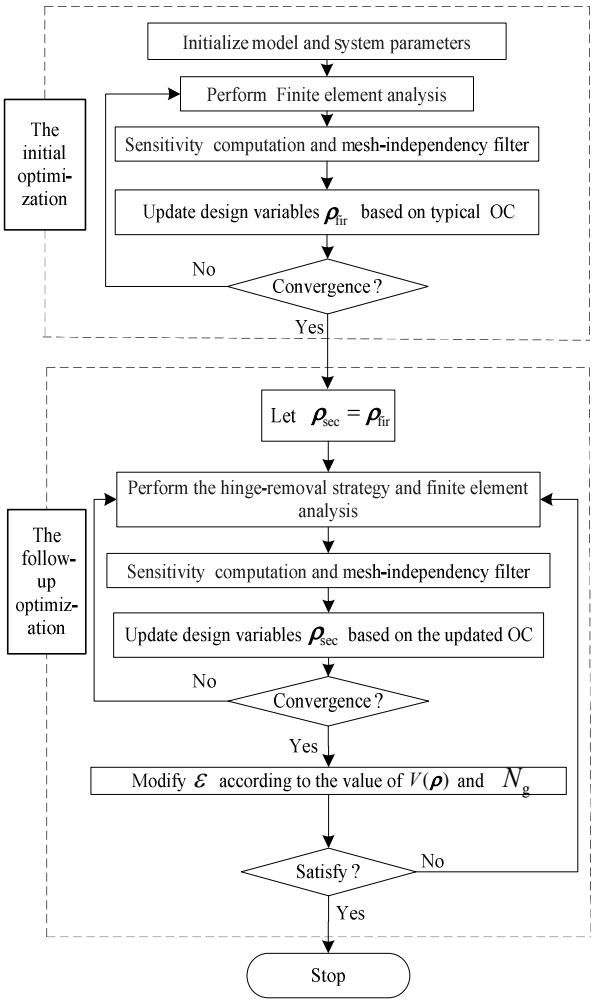

Fig. 2. Flow chart of the optimization approach for the black-and-white and hinge-removal topology design.

8. Numerical examples

8.1 A MBB beam

In the first example, the popular MBB beam which previously has been studied by many researchers [16, 19, 32, 33] is used to test the performance of the proposed approach for the black-and-white and hinge-removal topology design. The design domain and the boundary condition are sketched in Fig. 3. The dimension of the design domain is 6×1. The Young's modulus and Poisson's ratio are respectively $E=1$ and $v=0.3$. An input force $F_{in}=1$ is applied at the centre of the top edge. The volume fraction and filter radius are specified as 0.5 and 0.15, respectively [33]. Moreover, other parameters are given as $N_1=100$, $N_2=20$, $\delta_1=0.1$ and $\delta_2=1$. The optimization objective is to obtain the optimal topology of the MBB beam which minimizes the compliance.

This optimization problem is solved based on 180×30 4-node square element mesh discretization. Fig. 4 depicts the initial optimal topology based on the typical OC. It can be seen that grey boundaries inevitably appear in the topology plot, as seen in many topology design problems [20]. Subsequently, this solution is used as a starting point and then the follow-up optimization is implemented. To free unfavorable intermediate elements, the updated optimality criterion is thus employed to update design variables. And the hinge-removal strategy is also employed to check and circumvent potential one-point hinge connections. A set of optimal topologies with corresponding parameters are obtained, as shown in Fig. 5. Numerical solutions to the MBB beam are also listed in Table 1, wherein all the CPU time is based on a desktop computer with Intel(R) Core(TM) i7 870 processor of 2.93 GHz clock speed (the same hereinafter). Comparing Fig. 5 with Fig. 4, it can be seen that all final optimal topologies are markedly different from the initial one. Unfavorable grey regions are effectively removed and all members in topology solutions are plotted with a clear black-and-white and hinge-removal design

Table 1. The numerical solutions of the MBB beam with 180×30 mesh from the proposed approach.

α_0	$\Delta\alpha$	α_t	E_s	ε	V/V^0	N_g	k	T(s)
0.1	0.08	0.98	96.10	1e-9	0.5	6	341	840
0.1	0.1	0.9	96.16	1e-9	0.5	0	244	540
0.25	0.08	0.97	96.22	1e-9	0.5	0	263	600
0.25	0.1	0.85	96.42	1e-9	0.5	0	205	420
0.5	0.02	0.96	96.01	1e-12	0.5	0	545	$1.2\text{x}10^3$
0.5	0.04	0.98	96.13	1e-9	0.5	10	341	900

α_t : the terminal value of α ; $T(s)$: total CPU time.

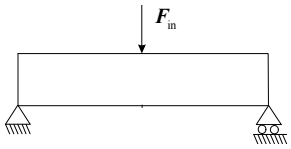

Fig. 3. Design domain of a MBB beam.

Fig. 4. The initial optimal topology of the MBB beam using the proposed approach with 180×30 mesh.

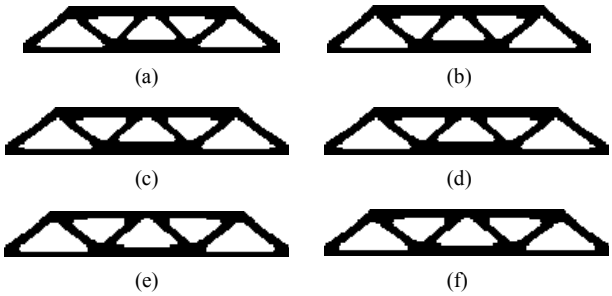

Fig. 5. The final optimal topologies of the MBB beam using the proposed approach with 180×30 mesh: (a) $\alpha_0=0.1$ and $\Delta\alpha=0.08$; (b) $\alpha_0=0.1$, $\Delta\alpha=0.1$; (c) $\alpha_0=0.25$, $\Delta\alpha=0.08$; (d) $\alpha_0=0.25$, $\Delta\alpha=0.1$; (e) $\alpha_0=0.5$, $\Delta\alpha=0.02$; (f) $\alpha_0=0.5$, $\Delta\alpha=0.04$.

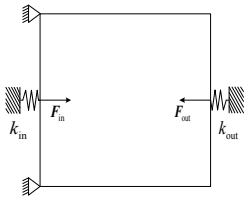

Fig. 6. Design domain of a force inverter.

pattern. The reason for this is that the updated optimality criterion formulated by slightly modifying OC enforces intermediate elements to be progressively removed from low to high density such that material can be added to the high-density elements. On the other hand, there is no one-point hinge connection to be found by tracking the optimization process. However, the implementation of the hinge-removal strategy has little influence on the CPU time. This is because the sensitivity calculations of the objective function become simple in this case.

Simultaneously, it can also be seen that final topologies in Fig. 5 and objective function values in Table 1 are relatively consistent and preserving the volume constraint. These show that the proposed approach is feasible for compliance minimum problems. Meanwhile, one can find that the continuation on α may result in a relatively large iteration number to achieve convergence. However, the increase in the total CPU time is moderate. This is because the present approach only requires computational complexity as low as possible.

8.2 A compliant force inverter

In the second example, the force inverter, which previously has been studied by Sigmund [32], is also employed to check the performance of the proposed approach for the black-and-white and hinge-removal topology design. As sketched in Fig. 6, the design domain, whose dimension is 120×120, is supported at the top and the bottom of the left edge. The Young's modulus is $E=1$ and Poisson's ratio $v=0.3$. An input force $F_{in}=1$ is applied at the centre of the left edge. The input and output springs are $k_{in}=1$ and $k_{out}=0.001$, respectively. And the volume fraction and filter radius are respectively specified as 0.25 and 2.5 [32]. Moreover, other parameters are given as $N_1=100$, $N_2=20$, $\delta_1=0.1$ and $\delta_2=1$. Due to the symmetry, only the lower half of the design domain is discretized with 4-node square element mesh. The optimization objective is to obtain the optimal topology of the force inverter which maximizes the stiffness and flexibility simultaneously.

This optimization problem is solved for different mesh densities, 120×60 and 180×90 elements. Fig. 7 depicts the symmetric halves of initial optimal topologies by using the typical OC. It can be seen that grey boundaries appear in the topology plot for each mesh. Then, by using each of them as a starting point respectively, the follow-up optimization is performed. Design variables are updated based on the updated

Table 2. The numerical solutions with different meshes from the proposed approach.

Mesh	α_0	$\Delta\alpha$	α_t	f_{sm}	ε	V/V^0	N_g	k	$T(s)$
120×60	0.2	0.025	0.975	-2.28	1e-6	0.25	0	903	4.08×10^3
	0.25	0.05	0.95	-2.28	1e-6	0.25	0	570	2.345×10^3
	0.4	0.02	0.94	-2.28	1e-6	0.25	0	836	3.548×10^3
180×90	0.2	0.025	1	-2.29	1e-6	0.25	0	922	16.81×10^3
	0.25	0.05	1	-2.29	1e-6	0.25	0	582	10.85×10^3
	0.4	0.02	1	-2.29	1e-6	0.25	2	882	25.92×10^3

α_t: the terminal value of α; $T(s)$: Total CPU time.

Fig. 7. The initial optimal topologies of the force inverter using the proposed approach with different meshes: (a) 120×60 mesh; (b) 180×90 mesh.

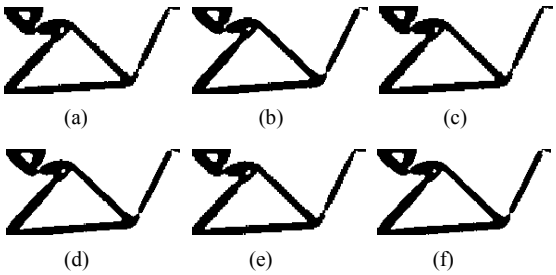

Fig. 8. The final optimal topologies of the force inverter using the proposed approach with different meshes: (a) 120×60 mesh, $\alpha_0=0.2$, $\Delta\alpha=0.025$; (b) 180×90 mesh, $\alpha_0=0.2$, $\Delta\alpha=0.025$; (c) 120×60 mesh, $\alpha_0=0.25$, $\Delta\alpha=0.05$; (d) 180×90 mesh, $\alpha_0=0.25$, $\Delta\alpha=0.05$; (e) 120×60 mesh, $\alpha_0=0.4$, $\Delta\alpha=0.02$; (f) 180×90 mesh, $\alpha_0=0.4$, $\Delta\alpha=0.02$.

OC and the hinge-removal strategy is used to prevent the one-point hinge connection. Fig. 8 and Table 2 depict the corresponding optimal topologies and numerical results with different meshes and varying parameters. As shown, black-and-white designs with appropriate parameters are obtained. Further, these topology layouts are free of one-point hinge connections and the minimum size of hinges is one-element-thick. Without doubt, black-and-white designs are contributed to the action of the optimality criterion formulated by slightly modifying OC. At the same time, the hinge-removal strategy can find the potential one-point hinge connections producing in the topologies and always circumvent them promptly. Besides, by combining Fig. 8 and Table 2, it can be seen that the optimal solutions are preserving the volume constraint and fairly consistent in both the resultant topologies and objective function values for the fixed mesh. These suggest that the proposed approach is also feasible for compliant mechanism problems. Moreover, one can find that the continuation on α requires a large iteration number to achieve convergence as

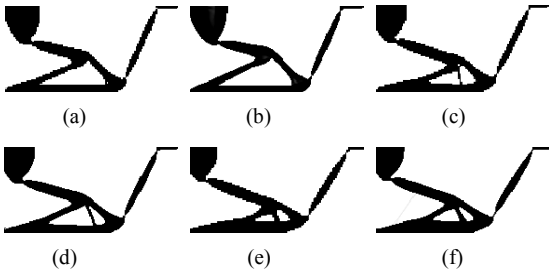

Fig. 9. Optimal topologies of the inverter with different meshes from the bilateral density filtering: (a) 120×60 mesh, $\Delta\sigma=0.002$; (b) 180×90 mesh, $\Delta\sigma=0.002$; (c) 120×60 mesh, $\Delta\sigma=0.005$; (d) 180×90 mesh, $\Delta\sigma=0.005$; (e) 120×60 mesh, $\Delta\sigma=0.01$; (f) 180×90 mesh, $\Delta\sigma=0.01$.

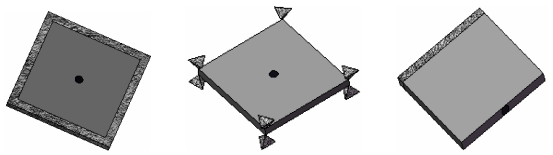

Fig. 10. Freely vibrating thin-plate structures (40 mm×40 mm×1 mm): (a) four edges clamped and concentrated mass m at the center of the structure (m = 0.3 m_s, m_s the total structural mass of the plate); (b) four corners supported and concentrated mass m at the center of the structure ($m = m_s$); (c) one edge clamped and concentrated mass m attached at the mid-point of the edge opposite to the clamped one ($m = m_s$).

well, whereas the increase in the total CPU time is still moderate, thanks to the low computation complexity of the proposed algorithm.

On the other hand, we compare the present approach with the bilateral density filtering proposed by Wang and Wang [33] for this example. The convergence criterion in Ref. [33], i.e. $|f^{k+1}-f^k|<10^{-5}$ or $|(\rho^a)^{k+1}-(\rho^a)^k|<10^{-6}$ (where ρ^a is the average density of non-empty elements) or $k>k_{\max}$, is adopted. Note that continuation strategies in which parameters σ_d and σ_r are chosen with relatively large values initially and then slowly decreased until the black-and-white optimum is obtained are used in their work. However, no specific details are given. Here, these two parameters are thus initialized as 1 and then gradually diminished until convergence with the fixed step $\Delta\sigma$ of -0.002, -0.005 and -0.01, respectively. The final optimal topologies and numerical results from the bilateral density filtering are shown in Fig. 9 and Table 3. Comparing them with Fig. 8 and Table 2, respectively, it can be seen that the proposed approach in this paper is slightly superior to the bilateral density filtering with parameters chosen in the 0-1 convergence, topology consistency and CPU time required.

8.3 Freely vibrating thin-plate structures

In the third example, freely vibrating thin-plate structures similar to Ref [43] are used to further verify the validity of the proposed method. As shown in Fig. 10, these thin-plate structures are with the same design domain of 40 mm×40 mm×40 mm, but three different cases of boundary conditions and attached concentrated, nonstructural masses. The material is isotropic with Young's modulus $E=10^{11}$ Pa, Poisson's ratio $v=0.3$ and mass density $\rho_m=78$ kg/m^3. And the volume fraction and filter radius are respectively specified as 0.5 and 1.5. For hinge detection parameters, δ_1 takes the value of 0.1, 0.7, and 0.1 respectively, while δ_2 is specified as 1. Moreover, N_1 is respectively given as 50, 60, 50, while N_2 is specified as 20. The optimization objective is to maximize the fundamental eigenvalue.

Table 3. The numerical solutions with different meshes from the bilateral density filtering.

Mesh	Δσ	f_{sm}	V/V^0	N_g	k	T(s)
120×60	-0.002	-2.2970	0.25	10	350	5.040x10^5
	-0.005	-2.1951	0.25	13	150	1.889x10^5
	-0.01	-1.9935	0.25	111	71	7.668x10^4
180×90	-0.002	-2.2983	0.25	229	350	2.604x10^6
	-0.005	-2.1781	0.25	7	148	1.101x10^6
	-0.01	-1.9687	0.25	71	89	4.806x10^5

T(s) : Total CPU time.

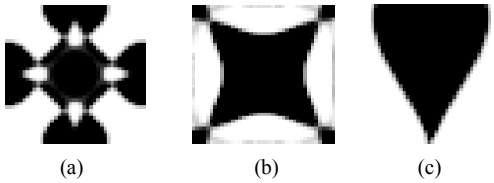

Fig. 11. The initial optimal topologies of freely vibrating thin-plate structures using the proposed approach with 40×40 mesh: (a) four edges clamped and m = 0.3 m_s; (b) four corners supported and $m = m_s$; (c) one edge clamped and $m = m_s$.

The design domains are all discretized using 4-node 40×40 plate elements. Based on the typical OC, the initial optimal topologies corresponding to these three cases are firstly obtained, as shown in Fig. 11. From this figure, it can be seen that intermediate design variables render the associated elements as gray. Therefore, each solution is used as a starting point and then the follow-up optimization is implemented to cure these problems in the topology layouts. The hinge-removal strategy and updated optimality criterion are applied in the optimization process.

Fig. 12 and Table 4 depict the optimal topologies and numerical results corresponding to parameters chosen. By comparing Fig. 12 with Fig. 11, it can be seen that resultant topologies from the proposed approach with appropriate parameters are almost truly 0-1 optimal designs satisfying the volume constraint. Clearly, this is due to the function of the updated optimality criterion. And by tracking the optimization process, the one-point hinge connection problem is found only in the case of four corners supported and concentrated mass at the center of the structure and is cured effectively as shown in Figs. 12(c) and (d). Again, it can be seen that final topologies

Table 4. The numerical solutions of freely vibrating structures with 40×40 mesh from the proposed approach.

Case	α_0	$\Delta\alpha$	α_t	ω_1	ε	V/V^0	N_g	k	T(s)
Four edges clamped	0.3	0.025	0.825	4506	1e-7	0.5	0	499	$1.74\text{x}10^3$
	0.5	0.02	0.52	4487	1e-6	0.5	0	102	308
Four corners supported	0.3	0.025	0.45	1058	1e-6	0.5	0	139	420
	0.5	0.02	0.52	1049	1e-6	0.5	0	109	305
One edge clamped	0.3	0.025	0.825	420	1e-10	0.5	0	519	$4.811\text{x}10^3$
	0.5	0.02	0.5	418	1e-6	0.5	0	100	603

α_t: The terminal value of α; T(s): Total CPU time.

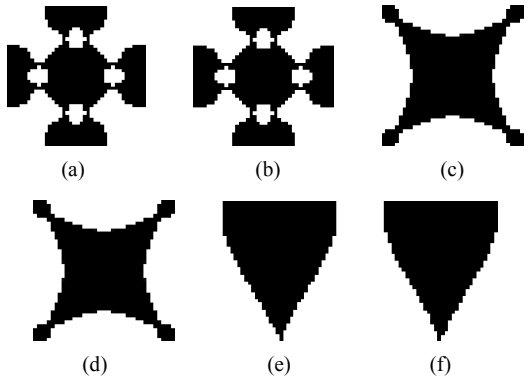

Fig. 12. Optimal topologies of freely vibrating thin-plate structures using the proposed approach with 40×40 mesh: (a) four edges clamped and $m = 0.3m_s$, $\alpha = 0.3$ and $\Delta\alpha = 0.025$; (b) four edges clamped and $m = 0.3m_s$, $\alpha = 0.5$ and $\Delta\alpha = 0.02$; (c) four corners supported and $m = m_s$, $\alpha = 0.3$ and $\Delta\alpha = 0.025$; (d) four corners supported and $m = m_s$, $\alpha = 0.5$ and $\Delta\alpha = 0.02$; (e) one edge clamped and $m = m_s$, $\alpha = 0.3$ and $\Delta\alpha = 0.025$; (f) one edge clamped and $m = m_s$, $\alpha = 0.5$ and $\Delta\alpha = 0.02$.

in Fig. 12 and objective function values in Table 4 are relatively consistent for the same boundary conditions and attached masses. At the same time, the optimized topologies are also preserving the volume constraint. These all indicate that the present approach is competent in producing expected black-and-white and hinge-removal designs for eigenvalue problems.

Moreover, one can still find that a large iteration number is required to achieve convergence due to the continuation on α for each boundary condition. The increase in the computational burden is however moderate, because only low computation cost is required by the proposed approach.

Further, for the purpose of comparison, the example of freely vibrating thin-plate structures is tested using the power-law OC-GSS algorithm proposed by Groenwold and Etman [19] again. The convergence criterion in Ref. [19], i.e. $||\boldsymbol{\rho}^{k+1}-\boldsymbol{\rho}^k|| < 10^{-6}$ or $k > 100$, is adopted. Optimal topologies and numerical results are respectively shown in Fig. 13 and Table 5, wherein notations $p_1 > 1$ respectively $q_1 > 1$ mean that continuation strategies described in Ref. [19] are employed. Comparing these results with Fig. 12 and Table 4, it can be seen that the power-law OC-GSS algorithm can also provide quasi 0-1 discrete solutions and is a bit more efficient in some cases than the present approach. However, topologies with different parameter values embody weak consistency for the same boundary condition. And one-point hinge connections are encountered in the topology layouts. From the latter, the proposed approach is slightly superior to the power-law OC-GSS algorithm.

Table 5. The numerical solutions of freely vibrating thin-plate structures with 40×40 mesh from OC-GSS algorithm.

Case	p_1	q_1	ω_1	V/V^0	N_g	k	$T(s)$
Four edges clamped	>1	>1	4452	0.5	8	100	309
	2	>1	4561	0.5	32	100	259
Four corners supported	>1	>1	1062	0.5	9	100	302
	2	>1	1063	0.5	27	100	318
One edge clamped	>1	>1	422	0.5	1	95	842
	2	>1	421	0.5	2	100	900

T(s): Total CPU time.

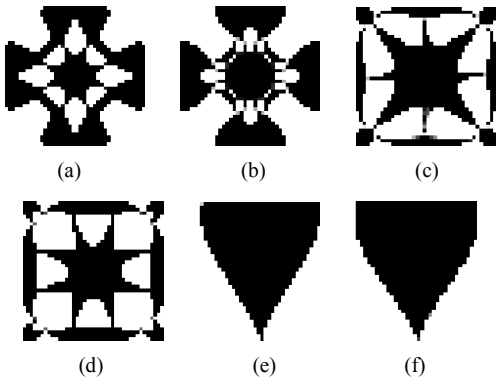

Fig. 13. Optimal topologies of freely vibrating thin-plate structures with 40×40 mesh using the power-law OC-GSS algorithm: (a) four edges clamped and $m = 0.3m_s$, $p_1 > 1$ and $q_1 > 1$; (b) four edges clamped and $m = 0.3m_s$, $p_1 = 2$ and $q_1 > 1$; (c) four corners supported and $m = m_s$, $p_1 > 1$ and $q_1 > 1$; (d) four corners supported and $m = m_s$, $p_1 = 2$ and $q_1 > 1$; (e) one edge clamped and $m = m_s$, $p_1 > 1$ and $q_1 > 1$; (f) one edge clamped and $m = m_s$, $p_1 = 2$ and $q_1 > 1$.

9. Conclusions

In this paper, an optimization approach for black-and-white

and hinge-removal topology designs is studied. To achieve this motive, an optimal topology allowing grey boundaries is found firstly. When a suitable design has been obtained, this solution is then used as a starting point for the follow-up optimization with the goal to free unfavorable intermediate elements. For this purpose, an updated optimality criterion in which a threshold factor is introduced to gradually suppress elements with low density is proposed. The typical optimality method and new technique proposed are applied to the design procedure sequentially. Besides, to circumvent the one-point hinge connection problem producing in the process of freeing intermediate elements, the hinge-removal strategy is also proposed. During the optimization, the binary constraints on design variables are relaxed based on the scheme of solid isotropic material with penalization. Meanwhile, the mesh-independency filter is employed to ensure the existence of a solution and remove well-known checkerboards. In this way, a solution that has few intermediate elements and is free of one-point hinge connections is obtained. Finally, different numerical examples including the compliance minimization, compliant mechanisms and vibration problems demonstrate the validity of the proposed approach.

Acknowledgment

This research was supported by the National Science Foundation of China (Grant No. 91223201), the National Natural Science Foundation of China (Grant No. 51275174), the United Fund of Natural Science Foundation of China and Guangdong province (Grant No. U0934004), Project GDUPS (2010), and the Fundamental Research Funds for the Central Universities (2012ZP0004). This support is greatly acknowledged.

References

[1] S. Bureerat and J. Limtragool, Performance enhancement of evolutionary search for structural topology optimisation, *Finite Elements in Analysis and Design*, 42 (2006) 547-66.

[2] B. Baumann and B Kost, Structure assembling by stochastic topology optimization, *Computers & Structures*, 83 (2005) 2175-84.

[3] G. Anagnostou and E. M. RHnquist and A. T. Patera, A computational procedure for part design, *Computer Methods in Applied Mechanics and Engineering*, 97 (1992) 33-48.

[4] C. Ghaddar, Y. Maday and A. T. Patera, Analysis of a part design procedure, *Numerische Mathematik*, 71 (1995) 465-510.

[5] M. Werme, Using the sequential linear integer programming method as a post-processor for stress-constrained topology optimization problems, *International Journal for Numerical Methods in Engineering*, 76 (2008) 1544-1567.

[6] K. Svanberg and M. Werme, Sequential integer programming methods for stress constrained topology optimization, *Structural and Multidisciplinary Optimization*, 34 (2007) 277-299.

[7] M. Beckers, Topology optimization using a dual method with discrete variables, *Structural Optimization*, 17 (1999) 14-24.

[8] C. S. Jog, A dual algorithm for the topology optimization of non-linear elastic structures, *International Journal for Numerical Methods in Engineering*, 77 (2009) 502-517.

[9] M. Stolpe and K. Svanberg, Modelling topology optimization problems as linear mixed black-and-white programs, *International Journal for Numerical Methods in Engineering*, 57 (2003) 723-739.

[10] M. Stolpe and T. Stidsen, A hierarchical method for discrete structural topology design problems with local stress and displacement constraints, *International Journal for Numerical Methods in Engineering*, 69 (2007) 1060-1084.

[11] M. P. Bendsøe and N. Kikuchi, Generating optimal topologies in structural design using a homogenization method, *Computer Methods in Applied Mechanics and Engineering*, 71 (1988) 197-224.

[12] S. Nishiwaki, M. I. Frecker, S. Min and N. Kikuchi, Topology optimization of compliant mechanisms using the homogenization method, *International Journal for Numerical Methods in Engineering*, 42 (1998) 535-559.

[13] M. P. Bendsøe and O. Sigmund, Material interpolation schemes in topology optimization, *Archive of Applied Mechanics*, 69 (1999) 635-654.

[14] C. B. W. Petersen, T. Buhl and O. Sigmund, Topology synthesis of large-displacement compliant mechanisms, *International Journal for Numerical Methods in Engineering*, 50 (2001) 2683-2705.

[15] G. I. N. Rozvany, Aims, scope, methods, history and unified terminology of computer-aided topology optimization in structural mechanics, *Structural and Multidisciplinary Optimization*, 21 (2001) 90-108.

[16] O. Sigmund, A 99 line topology optimization code written in Matlab. *Structural and Multidisciplinary Optimization*, 21 (2001) 120-127.

[17] M. P. Bendsøe, Optimal shape design as a material distribution problem, *Structural Optimization*, 1 (1989) 193-202.

[18] H. P. Mlejnik and R. Schirrmacher, An engineering approach to optimal material distribution and shape finding, *Computer Methods in Applied Mechanics and Engineering*, 106 (1993) 1-26.

[19] A. A. Groenwold and L. F. P. Etman, A simple heuristic for gray-scale suppression in optimality criterion-based topology optimization, *Structural and Multidisciplinary Optimization* (2009) DOI 10.1007/s00158-008-0337-1.

[20] M. P. Bendsøe and O. Sigmund, *Topology optimization*: *theory*, *methods*, *and applications*, Springer-Verlag, Berlin (2003).

[21] H. A. Eschenauer and N. Olhoff, Topology optimization of continuum structures: A review, *Applied Mechanics Reviews*, 54 (4) (2001) 331-390.

[22] R. B. Haber, A new approach to variable-topology shape design using a constraint on perimeter, *Structural Optimization*, 11 (1996) 1-12.

[23] J. Petersson and O. Sigmund, Slope constrained topology optimization, *International Journal for Numerical Methods in Engineering*, 41 (1998) 1417-1434.

[24] O. Sigmund, Design of material structures using topology optimization, *Ph.D. Thesis*, Department of Solid Mechanics, Technical University of Denmark, Denmark (2006).

[25] O. Sigmund, On the design of compliant mechanisms using topology optimization, *Mechanics of Structures and Machines*, 25 (4) (1997) 493-524.

[26] Y. Q. Fu and X. M. Zhang, Topology extraction in the topology optimization design for structures and compliant mechanisms, *Advances in Mechanics*, 36 (1) (2006) 75-84.

[27] Y. K. Sui, D. Q. Yang and B. Wang, Topological optimization of continuum structure with stress and displacement constraints under multipul loading cases, *Acta Mechanica Sinica*, 32 (2) (2000) 171-179.

[28] N. Kikuchi, S. Nishiwaki, J. S. O. Fonseca and E. C. N. Silva, Design optimization method for compliant mechanisms and material microstructure, *Computer Methods in Applied Mechanics and Engineering*, 151 (1998) 401-417.

[29] C.-Y. Lin and F.-M. Sheu, Adaptive volume constraint algorithm for stress limit-based topology optimization, *Computer-Aided Design*, 41 (2009) 685-694.

[30] T. Borrvall and J. Pertersson, Topology optimization using regularized intermediate density control, *Computer Methods in Applied Mechanics and Engineering*, 190 (2001) 4911-4928.

[31] M. Werme, Using the sequential linear integer programming method as a post-processor for stress-constrained topology optimization problems, *International Journal for Numerical Methods in Engineering*, 76 (2008) 1544-1567.

[32] O. Sigmund, Morphology-based black and white filters for topology optimization, *Structural and Multidisciplinary Optimization*, 33 (2007) 401-424.

[33] M. Y. Wang and S. Wang, Bilateral filtering for structural topology optimization, *International Journal for Numerical Methods in Engineering*, 63 (2005) 1911-1938.

[34] T. E. Bruns, A reevaluation of the SIMP method with filtering and an alternative formulation for solid-void topology optimization, *Structural and Multidisciplinary Optimization*, 30 (2005) 428-436.

[35] D. N. Chu, Y. M. Xie, A. Hira and G. P. Steven, Evolutionary structural optimization for problems with stiffness constraints. *Finite Elements in Analysis and Design*, 21 (1996) 239-251.

[36] M. Sauter, G. Kress, M. Giger and P. Ermanni, Complex-shaped beam element and graph-based optimization of compliant mechanisms, *Structural and Multidisciplinary Optimization*, 36 (2008) 429-442.

[37] N. P. Garcia-Lopez, M. Sanchez-Silva, A. L. Medaglia and A. Chateauneuf, A hybrid topology optimization methodology combining simulated annealing and SIMP, *Computers & Structures*, 89 (2011) 1512-1522.

[38] G.-W. Jang, M.-J. Kim and Y. Y. Kim, Design optimization of compliant mechanisms consisting of standardized elements, *ASME Journal of Mechanical Design*, 131 (2009) 121006-1-121006-8.

[39] Z. Luo, L. Y. Tong, M. Y. Wang and S. Y. Wang, Shape and topology optimization of compliant mechanisms using a parameterization level set method, *Journal of Computational Physics*, 227 (2007) 680-705.

[40] K. A. James and J. R. R. A. Martins. An isoparametric approach to level set topology optimization using a body-fitted finite-element mesh, *Computers & Structures*, 90-91 (2012) 97-106.

[41] N. F. Wang and K. Tai, Design of grip-and-move manipulators using symmetric path generating compliant mechanisms, *ASME Journal of Mechanical Design*, 130 (2008) 112305-1-112305-9.

[42] H. Zhou and K.-L. Ting, Geometric optimization of spatial compliant mechanisms using three-dimensional wide curves, *ASME Journal of Mechanical Design*, 131 (2009) 051002-1-051002-7.

[43] J. Du and N. Olhoff, Topological design of freely vibrating continuum structures for maximum values of simple and multiple eigenfrequencies and frequency gaps, *Structural and Multidisciplinary Optimization*, 34 (2007) 91-110.

[44] N. L. Pedersen, Maximization of eigenvalues using topology optimization, *Structural and Multidisciplinary Optimization*, 20 (2000) 2-11.

[45] X. M. Zhang, Topology optimization of compliant mechanisms, *Chinese Journal of Mechanical Engineering*, 39 (1) (2003) 47-51.

[46] M. I. Frecker, S. Kota and N. Kikuchi, Use of penalty function in topological synthesis and optimization of strain energy density of compliant mechanisms, *Proceedings of the 1997 ASME Design Engineering Technical Conferences*, DETC97/DAC-3760 (1997).

[47] M. I. Frecker, N. Kikuchi and S. Kotqa, Topology optimization of compliant mechanisms with multiple outputs, *Structural Optimization*, 17 (1999) 269-278.

[48] M. I. Frecker, G. K. Ananthasuresh, S. Nishiwaki and S. Kota, Topological synthesis of compliant mechanisms using multi-criteria optimization, *ASME Journal of Mechanical Design*, 119 (2) (1997) 238-245.

[49] M. I. Frecker and S. Canfield, Design of efficient compliant mechanisms from ground structure based optimal topologies, *Proceedings of the 2000 ASME Design Engineering Technical Conferences* DETC200/MECH-14142 (2000).

[50] G. K. Ananthasuresh, S. Kota and N. Kikuchi, Stratrgies for systematic synthesis of compliant MEMS, *Proceedings of the 1994 ASME Winter Annual Meeting on Dynamic Systems and Control*, IL, Chicago, DSC 55 (2) (1994) 677-686.

[51] J. A. Hetrick and S. Kota, Topological and geometric synthesis of compliant mechanisms, *Proceedings of the 2000 ASME Design Engineering Technical Conferences* DETC200/MECH-14140 (2000).

[52] M. Bendsøe, *Optimization of structural topology, shape and material*, Springer-Verlag, Berlin (1995).

[53] X. M. Zhang, Optimal design of flexible mechanisms with frequency constraints, *Mechanism and Machine Theory*, 30

(1) (1995) 131-139.
[54] X. M. Zhang, Integrated optimal design of flexible mechanism and vibration control. *International Journal of Mechanical Sciences*, 46 (2004) 1607-1620.
[55] K. T. Zuo, Research of theory and application about topology optimization of continuum structure, *Ph.D. Thesis*, Huazhong University of Science and Technology, Wuhan, China (2004).

Yongqing Fu received her Ph.D. in Mechanical Engineering from South China University of Technology, China, in 2009. She is an associate professor in the School of Design of South China University of Technology, China. Her research interests include topology optimization and topology extraction.